Numerical study on energy and exergy performances of a microencapsulated phase change material slurry based photovoltaic/thermal module

Yu, Qinghua; Romagnoli, Alessandro; Yang, Ren; Xie, Danmei; Liu, Chuanping; Ding, Yulong; Li, Yongliang

DOI:
10.1016/j.enconman.2019.01.029

Numerical study on energy and exergy performances of a microencapsulated phase change material slurry based photovoltaic/thermal module

Qinghua Yu[a, b], Alessandro Romagnoli[c], Ren Yang[a], Danmei Xie[b], Chuanping Liu[d], Yulong Ding[a], Yongliang Li[a,*]

[a] Birmingham Centre for Energy Storage, School of Chemical Engineering, University of Birmingham, Birmingham B15 2TT, United Kingdom

[b] Key Laboratory of Hydraulic Machinery Transients (Wuhan University), Ministry of Education, Wuhan 430072, China

[c] School of Mechanical and Aerospace Engineering, Nanyang Technological University, Singapore 639798, Singapore

[d] School of Energy and Environmental Engineering, University of Science and Technology Beijing, Beijing 100083, China

[*]Corresponding author. Tel.: +44 (0) 121 414 5135, Email: y.li.1@bham.ac.uk (Y. Li)

Abstract

Microencapsulated phase change material (MPCM) slurry has proven to have potential in elevating the overall performance of a photovoltaic/thermal (PV/T) module as a working fluid. In order to make full use of the superiority of MPCM slurry and further improve energy and exergy efficiencies of the PV/T module, the effects of MPCM concentration and melting temperature under a wide inlet fluid velocity range were explored based on a three-dimensional numerical model of coupled heat transfer in this study. The results show that both the energy and exergy efficiencies increased with the concentration. A lower melting temperature resulted in higher energy efficiency, whereas a higher melting temperature is helpful for exergy efficiency improvement. The slurry with an excessively low melting temperature (e.g. 27°C) even led to lower exergy efficiency than pure water. The melting temperature needs to be precisely tailored to make a compromise between energy and exergy efficiencies. In comparison with pure water, the improvement in energy efficiency provided by the slurry was further enhanced at a lower inlet velocity, while the improvement in exergy efficiency was optimized by adjusting the inlet velocity to a certain value. The maximum improvement in energy efficiency provided by the slurry was 8.3%, whilst that in exergy efficiency was 3.23% in this work. From the above, the superiority of MPCM slurry can be further promoted by selecting suitable material properties and operating parameters.

Keywords: Photovoltaic/thermal module; Microencapsulated phase change material; Heat transfer; Numerical simulation; Exergy efficiency.

Nomenclature

$\boldsymbol{A}$	area, m^2	λ	thermal conductivity, W/m K
c	volumetric concentration	ΔT_r	melting temperature range, K
c_p	specific heat, J/kgK	*Subscripts*	
d	diameter, m	a	ambient or wind
e	shear rate, 1/s	AP	absorber plate
$\dot{Ex}$	exergy, W	b	bulk fluid
h	heat transfer coefficient, W/m^2K	c	convection
L_p	latent heat, kJ/kg	e	electrical
p	pressure, Pa	ex	exergy
P	packing factor	f	carrier fluid or flow
Pe_p	particle Peclet number	h	heat transfer
q	heat flux, W/m^2	in	inlet
Q_S	solar radiation intensity, W/m^2	l	liquid
$\dot{S}_{gen}$	volumetric entropy generation rate, W/m^3K	m	melting
T	temperature, K	out	outlet
$\vec{u}$	velocity vector, m/s	p	particle
V	volume, m^3	PV	PV panel
Greek		$\boldsymbol{ref}$	reference
α	absorptivity or thermal diffusivity, m^2/s	s	solid
β	temperature coefficient, 1/K	t	total or tube
ε	emissivity	th	thermal
η	efficiency	*Abbreviations*	
μ	viscosity, Pa·s	PV/T	photovoltaic/thermal
ρ	Density, kg/m^3	HTF	heat transfer fluid
σ_{sb}	Stefan-Boltzmann constant, W/m^2K^4	MPCM	microencapsulated phase change material

1. Introduction

The energy supply strategy is irreversibly shifting from conventional fossil fuels to clean renewable energy sources to tackle energy shortage and environmental problems. Solar energy, as one of the promising renewable energy sources, has had an increasing market share in the last few years. The solar cell is currently the most prevalent solar energy power conversion device since it can directly convert solar radiation into high-grade electrical energy. However, a photovoltaic (PV) panel consisting of solar cells exhibits a notable temperature rise as it is exposed to solar radiation [1], which causes PV efficiency degradation and electrical power output loss [2]. Specifically, PV efficiency would decrease by about 0.5% as the temperature of the crystalline silicon cells increased by 1℃ [3]. In order to prevent PV efficiency degradation, a cooling fluid is usually adopted to circulate at the back of a PV panel, which could remove generated heat and make the PV panel operate at lower temperatures [4]. The heat captured by the cooling fluid can also be further utilized. Such a conversion system of solar energy, simultaneously producing electricity and heat from solar radiation, is known as a photovoltaic/thermal (PV/T) system. PV/T systems have proven to exhibit greater energy output per unit installation area and larger total energy efficiency, compared to a PV panel or a conventional solar thermal collector [5].

Except for the geometrical configuration studied by Shan et al. [6], the type of heat transfer fluid (HTF) or working fluid is another crucial factor in determining the performance or efficiency of PV/T systems [7]. The HTFs used in PV/T systems which are widely investigated in the literature mainly include air, water, and nanofluids [8]. Farshchimonfared et al. [9] carried out optimum designs of an air-based PV/T collector connected to distribution ducts of heated air. Solanki et al. [10] also explored the performance of an air-based PV/T system. They demonstrated that maximum electrical and thermal efficiencies achieved by the system were around 8% and 39%, respectively. Dimri et al. [11] integrated a thermoelectric cooler into an air-based PV/T module, which obtained an increase by 7.3% in overall electrical efficiency and an increase of 0.8%-2% in overall exergy efficiency compared with conventional PV collector. Habibollahzade et al. [12] combined air-based PV/T panels and a solar chimney to augment exergy efficiency and power generation. Their study indicated that the proposed system exhibited higher exergy efficiency at a lower PV/T panel temperature and a total exergy efficiency of 3.3% was obtained under a good balance with cost rate by multi-objective optimization. The inferior heat removal ability of air becomes the major issue of an air-based system, which is attributed to the weak thermal conductivity, small density and low specific heat of air. Compared with air, water enhanced heat removal ability, and thus in the water-based PV/T system, both the electrical and thermal efficiencies were elevated. A typical water-based system proposed by Huang et al. [13] reached a thermal efficiency of about 50% and an electrical efficiency of about 9.5%. Aste et al. [14] designed a thin film PV/T collector using water as HTF and simulated its performance using a one-dimensional mathematical model. They reported that the average annual overall efficiency of the designed collector was about 42%. Kuo et al. [15] employed the Taguchi method to optimize control parameters of a water-based PV/T collector for simultaneously improving electrical and thermal efficiencies, which were 14.29% and 44.96% after optimization respectively. Mousavi et al. [16] reported that integration of phase change materials in a porous medium with a water-based PV/T collector could reach a highest thermal efficiency of 83% as well as an exergy efficiency of 16.7% under a solar irradiance of 600 W/m^2. Thinsurat et al. [17] proposed a water-based PV/T system integrated with thermal storage units of thermochemical sorption, which could serve as a sole hot water supplier for a typical household in an entire year. The proposed system could also achieve an electric efficiency of 13% and reduce the annual consumption of electricity to half at least. Introducing nanofluids in PV/T systems can further improve energy efficiency due to the increased thermal conductivity compared to pure water. Sardarabadi et al. [18] explored the role of SiO_2-water nanofluid in a PV/T module and their study indicated that utilization of 3 wt.% nanoparticles led to an increase by 7.9% in overall energy efficiency with respect to pure water. It should be noted that energy efficiency does not always increase with the nanoparticle concentration mainly due to the reduction of average specific heat of nanofluids [19]. Khanjari et al. [20] comparatively analyzed the performances of tube-plate PV/T systems using pure water, Al_2O_3-water nanofluid, and Ag-water nanofluid as HTFs. They concluded that the energy and exergy efficiencies, as well as heat transfer coefficient, were all increased by introducing nanofluids whilst the Ag-water nanofluid offered preferable improvement. Lari et al. [21] designed an Ag-water nanofluid-based PV/T module to supply electricity and heat for residential applications. Their economic analysis indicated that the proposed system reduced the energy cost by 82% compared with the domestic electricity price in Saudi Arabia. Rahbar et al. [22] established a 1-D model to study a novel concentrating PV/T collector with Ag-water nanofluid as HTFs and triple-junction InGaP/InGaAs/Ge as PV cells. Their work demonstrated that it outperformed a collector without nanofluid with a value of 5.1% in the overall energy efficiency. They also proposed to couple it with organic Rankine cycle for further increasing system performance. Bellos et al. [23] examined a PV/T collector with a parabolic concentrator using pure oil or CuO-oil nanofluid as HTFs under various combinations of inlet temperature and volumetric flow rate. They found that the nanofluid provided enhancements of 2.08% and 3.05% in the total energy and exergy efficiencies, respectively, compared to pure oil at a volumetric flow rate of 540 L/h with an inlet temperature of 100°C.

Similar to nanofluids, a microencapsulated phase change material (MPCM) slurry can be formed by uniformly dispersing small enough MPCM particles (i.e. PCM microcapsules) and making them suspended in a carrier liquid (such as water) [24]. Because of MPCM latent heat as well as the interaction among the MPCM particles, carrier liquid and tube wall, the resulting MPCM slurry generally has large apparent specific heat and enhanced heat transfer ability. The MPCM slurry thus has a strong ability to absorb and store large amounts of thermal energy with a decent heat transfer coefficient [25]. Furthermore, the MPCM melting temperature can be specified or selected to fit specific application [26]. In addition, the flow rate of MPCM slurry can be easily regulated in light of its decent flowability. The above advantages or features justify that the MPCM slurry seems to be a promising alternative for conventional working fluids such as water to play a role in PV/T systems.

At a fundament level, a volume of work has been conducted on the heat transfer behavior of MPCM slurries in various channels and heat exchangers [27]. At the application level, much work has also been carried out on the use of MPCM slurries in building heating [28] and heat storage [29]. Recently, several researchers have explored the utilization of MPCM slurries in PV/T systems. Qiu et al. theoretically [30] and experimentally [7] examined the performance of a novel PV/T system with MPCM slurry as HTF but without exergy analysis. Moreover, the theoretical analysis based on energy conservation and experimental tests based on local monitoring cannot offer clear and deep insight into the effects of heat transfer, flow and phase change behavior of MPCM slurries on the PV/T system performance. Liu et al. [31] adopted a two-dimensional numerical model to analyze the dynamic performance of a dual channel PV/T module with MPCM slurry and air as HTFs. In their model, they did not take into account heat transfer enhancement caused by the micro-convection of particles. The results showed that the designed collector with MPCM slurry exhibited the highest overall energy efficiency of 80.57% at 13:00 while its overall exergy efficiency achieved a maximum value of 11.4% in the morning. Liu et al. [32] also set up a three-dimensional numerical model to evaluate the performance of a novel miniature concentrating PV/T collector using MPCM slurry as HTF. They stated that lower solar radiation intensity would result in higher electrical efficiency and higher thermal efficiency. The above studies proved that the utilization of MPCM slurry simultaneously elevated the electrical and thermal efficiencies of a PV/T collector compared to pure water.

However, the effect of MPCM melting temperature as a key parameter on the performance of a PV/T module remains unaddressed in the literature, and thus it is unclear how to select suitable MPCM. Furthermore, exergy analysis for the MPCM slurry based PV/T module is scarce in the literature, whilst the phase change of MPCM leads to distinct exergy characteristics. In addition, another two key parameters, MPCM volumetric concentration and inlet slurry velocity, can both influence the melting region distribution of MPCM slurry in tubes, which determine the effectiveness of slurry in performance improvement of a PV/T module. Nevertheless, a study on the combined effects of the two key parameters cannot be found in the literature, except that the effects of the two key parameters have been separately explored [31]. The present study attempts to figure out the above-mentioned issues to make full use of the superiority of MPCM slurry and further improve the electrical, thermal and exergy efficiencies of a PV/T module. A three-dimensional numerical model of coupled heat transfer including the forced convection of slurry, convection of surrounding air, thermal radiation and thermal conduction, was established to evaluate the performance of MPCM slurry based PV/T modules. The numerical model was developed in commercial software, Fluent, and validated by comparing the resulting data with previous experimental and numerical studies. A series of simulations were performed on the basis of the validated model to predict the temperature distributions of a PV/T module under different key parameter combinations, which were then used to discern the role of MPCM in heat transfer. The pure water was also selected as a working fluid as a baseline for comparison. On the basis of the simulation results, the comprehensive performances of the module were calculated and compared, which included electrical, thermal and primary-energy saving efficiencies as well as exergy efficiency. The comprehensive performance enhancements of the PV/T module were elaborated after introducing the MPCM slurry compared with pure water. This study is helpful to understand in depth the performance of MPCM slurry based PV/T modules.

2. Numerical model and solving procedure

2.1. Model geometry and main assumptions

The proposed PV/T module in this study comprises a PV panel, an absorber plate, five identical tubes and a thermal insulation layer, as shown in Fig. 1. The PV panel was placed on the upper surface of the absorber plate while the five tubes were evenly welded on the back surface of the absorber plate. All surfaces of the PV/T collector except the upper surface were covered by the thermal insulation layer. In order to economize computational time and resources, only 1/5 of the absorber plate and one tube were selected as the computational domain [20]. The effects of the PV panel and thermal insulation layer were considered in the boundary conditions. Dimensions and materials of the tubes, absorber plate and PV panel are gathered in Table 1.

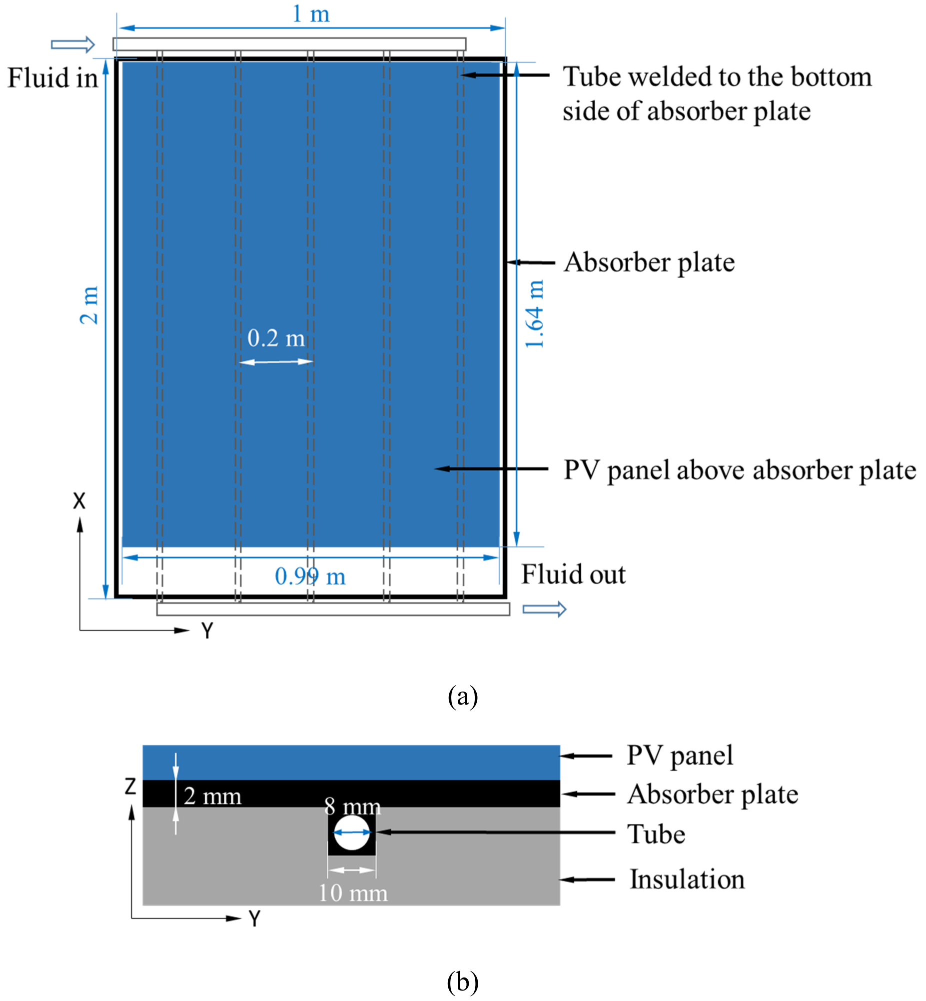

Fig. 1 Schematic of PV/T module: (a) front view and (b) local cross section (1/5).

Table 1 Dimensions, materials and properties for different components of the module [5].

Tubes	Absorber plate	PV panel
Number: 5	Length: 2 m	Length: 1.64 m
Length: 2 m	Width: 1 m	Width: 0.99 m
Outlet diameter: 0.01 m	Thickness: 0.002 m	α_{PV}=0.9
Wall thickness: 0.001 m	Material: copper	ε_{PV}=0.88
Spacing between center of tubes: 0.2 m	α_{AP}=0.95	η_{ref}=12% at T_{ref}=25 °C
Material: copper (ρ=8978 kg/m^3, λ=387.6 W/m K, c_p=381 J/kg K)	ε_{AP}=0.05	β=0.0045 °C^{-1}

The numerical model of coupled heat transfer was established on the basis of the following main assumptions: (a) because the MPCM particles are small enough and can uniformly disperse in the carrier fluid, the MPCM slurry can be considered homogeneous and can be treated as a single phase fluid [27], which has been repeatedly adopted in the literature [33]; (b) the slurry shows Newtonian behavior as the MPCM volumetric concentration is less than 25% [34], which has also been proved by experimental measurements of the slurry viscosity [35]; (c) effective thermal conductivity is adopted for the micro-convection stemming from the interactions of particles with carrier fluid and tube wall [34]; (d) the melting process occurs over a temperature range with a width of ΔT_r across the melting temperature T_m, and the lower and upper melting temperature limits are assumed to be $T_L = T_m - \frac{1}{2}\Delta T_r$ and $T_H = T_m - \frac{1}{2}\Delta T_r$, respectively [36]; (e) the flow is laminar, steady-state, incompressible, and fully developed at the outlet; (f) the inlet velocities of all tubes are the same; (g) solar radiation is normal to the upper surface of the PV panel or the absorber plate; (h) all the surfaces of the absorber plate and tube contacting with the thermal insulation layer are considered adiabatic; (i) the back surface of the PV panel perfectly contacts with the upper surface of the absorber plate and thus the temperature distribution is regarded as the same in the two layers.

2.2. Governing equations and boundary conditions

The equations governing the laminar flow and thermal convection in the fluid region include continuity, momentum and energy equations, which can be expressed as

$$\nabla \cdot \vec{u} = 0, \tag{1}$$

$$\nabla \cdot (\rho_b \vec{u}\vec{u}) = -\nabla p + \mu_b \nabla^2 \vec{u} + \rho_b \vec{g}, \tag{2}$$

$$\nabla \cdot \left(\rho_b \vec{u} c_{pb} T\right) = \nabla \cdot (\lambda_b \nabla T). \tag{3}$$

The governing equation for the thermal conduction in the solid region is

$$\nabla \cdot (\lambda_s \nabla T) = 0. \tag{4}$$

The solar radiation is captured to produce electricity and heat. The latter is then partially dissipated into the surroundings by ambient radiation and air convection while the rest is transferred into the HTF through the absorber plate. Therefore, the absorbed net heat flux on the upper surface of the absorber plate covered by the PV panel can be calculated by [1]

$$q_{AP} = Q_S(\alpha_{PV} - \eta_e) - \varepsilon_{PV}\sigma_{sb}(T_{PV}^4 - T_a^4) - h_c(T_{PV} - T_a), \quad (5)$$

where σ_{sb} = 5.67×10^{-8} W/m^{2}K^4 and $h_c = 3u_a + 2.8$ [37]. In this study, the ambient conditions were set as $Q_S = 1000$ W/m^2, T_a= 273.15 K and u_a = 0.5 m/s [5]. Similarly, the absorbed net heat flux on the upper surface of the absorber plate not covered by the PV panel can be calculated by

$$q_{AP} = Q_S\alpha_{AP} - \varepsilon_{AP}\sigma_{sb}(T_{AP}^4 - T_a^4) - h_c(T_{AP} - T_a). \quad (6)$$

All the surfaces contacting the thermal insulation are set to adiabatic boundaries. The two side surfaces of the segmental absorber plate are set to symmetric boundaries. The boundary conditions for the HTF flow are presented in Table 2.

Table 2 Boundary conditions for the HTF flow.

At the tube inlet	At the tube outlet	At the inner surface of the tube
u_x=u_{in}	p=p_a(static pressure)	$u_x = u_y = u_z = 0$
$u_y = u_z = 0$		$q_f = q_t$
T=$T_{in} = T_a$		$T_f = T_t$

2.3. Properties of working fluids

The carrier fluid in this study was pure water. The temperature-dependent thermo-physical properties of pure water can be found in Reference [20]. The hydrocarbon n-eicosane was selected as PCM while the TiO_2 was selected as shell material in this study. The weight of PCM core accounted for about 78% of a microcapsule. The properties of PCM microcapsules are summarized in Table 3 [38]. Based on the assumption (a), the bulk properties of the MPCM slurry can be calculated as a combination of the properties of the MPCM particles and carrier fluid by various theoretical homogeneous models and experimental correlations [36]. Based on the mass balance, the slurry density is expressed as

$$\rho_b = c\rho_p + (1 - c)\rho_f. \tag{7}$$

Table 3 The properties of n-eicosane microcapsule in this study [38].

Density (kg/m^3)	Specific heat (J/kg K)	Latent heat (kJ/kg)	Thermal conductivity (W/m K)	Melting point (°C)	Particle Size (μm)
946.4	1973.1	192.66	0.749	37	10

The slurry dynamic viscosity can be calculated using the following correlation which has been validated for a particle concentration of up to 20% [39]:

$$\mu_b = (1 - c - 1.16c^2)^{-2.5}\mu_f. \tag{8}$$

The static thermal conductivity of the bulk slurry can be calculated based on the Maxwell model [36] as

$$\lambda_b = \lambda_f \frac{2 + \lambda_p/\lambda_f + 2c(\lambda_p/\lambda_f - 1)}{2 + \lambda_p/\lambda_f - c(\lambda_p/\lambda_f - 1)}. \tag{9}$$

When the slurry is flowing, the micro-convection mentioned in the assumption (c) will increase the effective thermal conductivity of the slurry, of which the calculated correlation can be found in Reference [34].

On the basis of the energy balance, the bulk specific heat of the slurry can be piecewise written as [36]

$$c_{pb} = \begin{cases} \left[c\left(\rho c_{p,s}\right)_p + (1-c)\left(\rho c_p\right)_f\right]/\rho_b & \text{for } T < T_L \\ \left[c\left(\rho\left(\frac{c_{p,s}+c_{p,l}}{2} + \frac{L_p}{T_l - T_s}\right)\right)_p + (1-c)\left(\rho c_p\right)_f\right]\Big/\rho_b & \text{for } T_L \le T \le T_H \\ \left[c\left(\rho c_{p,l}\right)_p + (1-c)\left(\rho c_p\right)_f\right]/\rho_b & \text{for } T > T_H \end{cases} \quad (10)$$

This equation accounts for the phase change of the MPCM particles in the melting range between T_L and T_H as a step function. The melting temperature range ($\Delta T_r = T_H$-T_L) is set as 1 K in this study [36].

2.4. Energy and exergy analysis

The gained thermal energy of the HTF equals the absorbed net heat on the upper surface of the absorber plate. Therefore, the thermal efficiency of the PV/T module according to the first thermodynamic law can be written as

$$\eta_{th} = \frac{\int_{A_{AP}} q_{AP} dA}{Q_S A_{AP}}, \quad (11)$$

The electrical efficiency of the PV panel depends on its temperature, which can be expressed as [3]

$$\eta_e = \eta_{ref}\left[1 - \beta\left(T_{PV} - T_{ref}\right)\right]. \quad (12)$$

In order to reflect the high grade characteristics of electrical energy, primary-energy saving efficiency is proposed to indicate the overall energy performance of the PV/T module [40], which is defined as

$$\eta_p = \eta_{th} + P\,\eta_e/\eta_{power}. \quad (13)$$

Here *P* denotes the area ratio of the PV panel to the absorber plate; $\eta_{power} = 38\%$, denoting the general efficiency of a conventional thermal power plant;

The exergy efficiency of the PV/T module can be expressed as

$$\eta_{ex} = \dot{Ex}_{gain}/\dot{Ex}_{input} = \left(\dot{Ex}_e + \dot{Ex}_{th}\right)/\dot{Ex}_{solar}, \quad (14)$$

The electrical exergy equals the produced electrical energy, which can be written as

$$\dot{Ex}_e = \eta_e Q_S A_{PV}. \tag{15}$$

The thermal exergy obtained by the HTF can be calculated by

$$\dot{Ex}_{th} = \int_{A_{AP}} q_{AP}\left(1 - \frac{T_a}{T}\right) dA - \int_{V_{fluid}} T_a\left(\dot{S}_{gen,h} + \dot{S}_{gen,f}\right) dV, \tag{16}$$

where $\dot{S}_{gen,h}$ and $\dot{S}_{gen,f}$ are the local volumetric entropy generation rates stemming from irreversible heat transfer and flow friction in the HTF, which can be obtained by [41]

$$\dot{S}_{gen,h} = \frac{\lambda_b}{T^2}\left[\left(\frac{\partial T}{\partial x}\right)^2 + \left(\frac{\partial T}{\partial y}\right)^2 + \left(\frac{\partial T}{\partial z}\right)^2\right], \tag{17}$$

$$\dot{S}_{gen,f} = \frac{\mu_b}{T}\left[2\left(\frac{\partial u}{\partial x}\right)^2 + \left(\frac{\partial u}{\partial y}\right)^2 + \left(\frac{\partial u}{\partial z}\right)^2\right]. \tag{18}$$

The calculation of the solar radiation exergy ($\boldsymbol{\dot{Ex}_{solar}}$) can be found in Reference [20].

3. Numerical method and model validation

In this study, the governing equations mentioned in Section 2.2 were solved by the commercial software, Fluent, based on the finite volume method. The SIMPLE algorithm was selected to tackle the pressure-velocity coupling. The gradients of solved variables at the control volume center were calculated through the Green-Gauss cell-based method. The discretizing of convection and diffusion terms in momentum and energy equations was accomplished based on the QUICK scheme. As the residual values of continuity, momentum and energy equations reduced below 10^{-6}, 10^{-6} and 10^{-9} respectively, the numerical solution was regarded as convergent. The whole computational domain was discretized by structured hexahedral cells. The resulting grid from the Y-Z view with the locally enlarged image is illustrated in Fig. 2(a) while the grid on the local A-A section of the X-Z view is shown in Fig. 2(b). The grids are refined in the fluid region near the solid/fluid interfaces where velocity and temperature gradients are large. In order to carry out the test of grid independence, simulation results on the basis of three different grid sets with 630,000, 890,000 and 1,120,000 cells were comparatively analyzed. The predicted average absorber plate temperature, average tube outlet temperature and pressure drop in the tube under the three grid sets are summarized in Table 4. It can be found from this table that the differences in the average temperatures of the absorber plate and tube outlet are both less than ±0.3 K and the percentage difference in the pressure drop is below 0.35% between the third and second grid sets. Hence, the following numerical simulations in this study were performed under the third grid set (i.e. 1,120,000 cells).

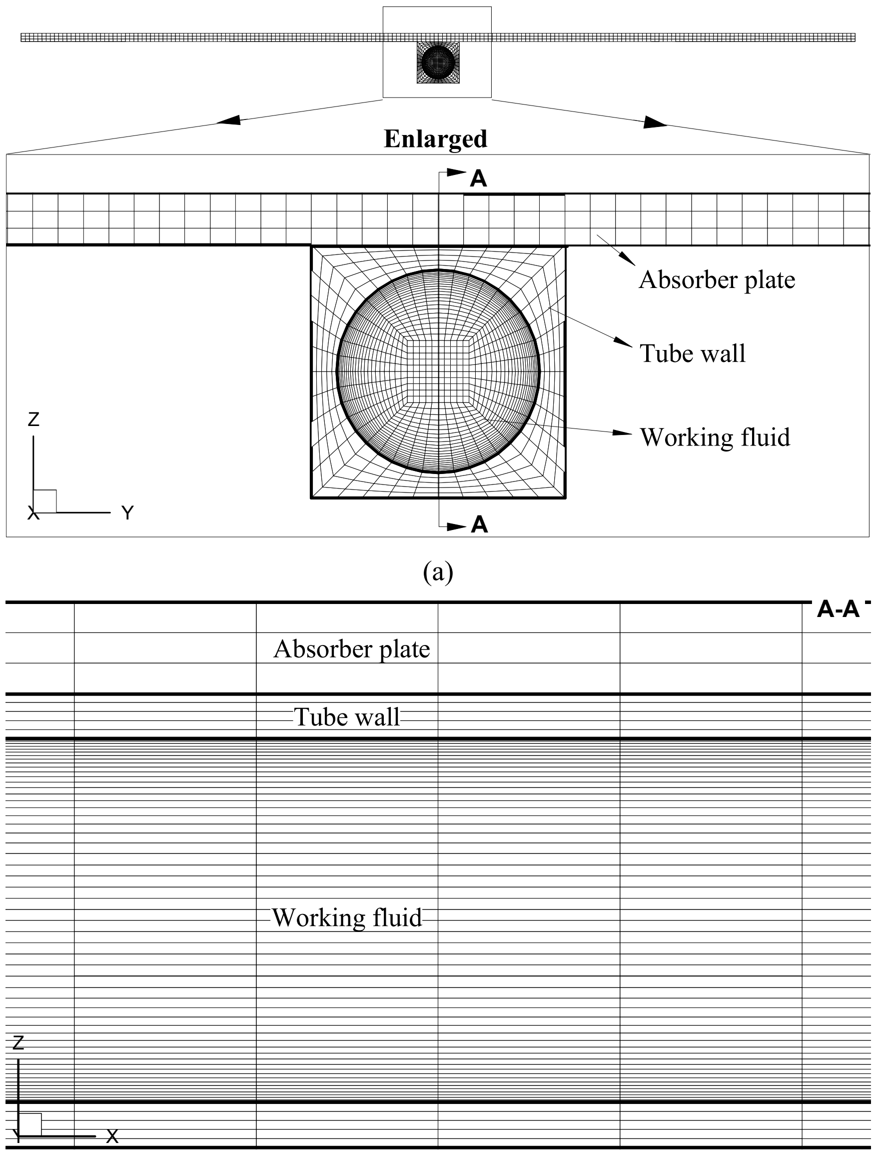

(b)

Fig. 2 Computational domains and grids: (a) Y-Z view and (b) Local A-A section of X-Z view.

Table 4 Results of grid-independent test for the average absorber plate temperature ($\bar{T}_{AP}$), average tube outlet temperature ($\bar{T}_{out}$) and pressure drop (Δp) at a slurry with c=10% and u_{in}=0.1 m/s.

Grid number	$\bar{T}_{AP}$ (K)	Difference (K)	$\bar{T}_{out}$ (K)	Difference	Δp (Pa)	Difference (%)
630,000	315.11	-	308.72	-	98.41	-
890,000	316.23	1.02	309.55	0.83	102.95	4.6
1,120,000	316.49	0.26	309.76	0.21	103.32	0.35

The established model was validated from two aspects. In the first aspect, the temperature data of a water-cooled PV/T system calculated by the established model was compared with one similar simulation work [20], as shown in Fig. 3(a). It can be seen that they have the same trend and little difference of less than 1 K at the same conditions, which shows a decent agreement. In the second aspect, the comparison was carried out with the experimental data on the convective heat transfer of MPCM slurry flow in a circular duct with a diameter of 3.14 mm [42] and 4 mm [35]. As presented in Fig. 3(b), the duct wall temperature predicted by the established model was compared with the experimental data for Stefan number of 3 (Ste = 3) [42]. It can be observed that the predicted wall temperatures coincide with the experimental data. Fig. 3(c) compares the Nusselt number predicted by this model with the experimental data [35] for two combinations of Reynolds number (Re) and Stefan number (Ste). It is obvious that the predicted Nusselt number agrees well with the experimental data at both two combinations. The heat transfer within a water-based PV/T module and the heat transfer of MPCM slurry in a duct involve all heat transfer processes in the MPCM slurry based PV/T module proposed in this paper. From the above, the established model proves to be reasonable and valid.

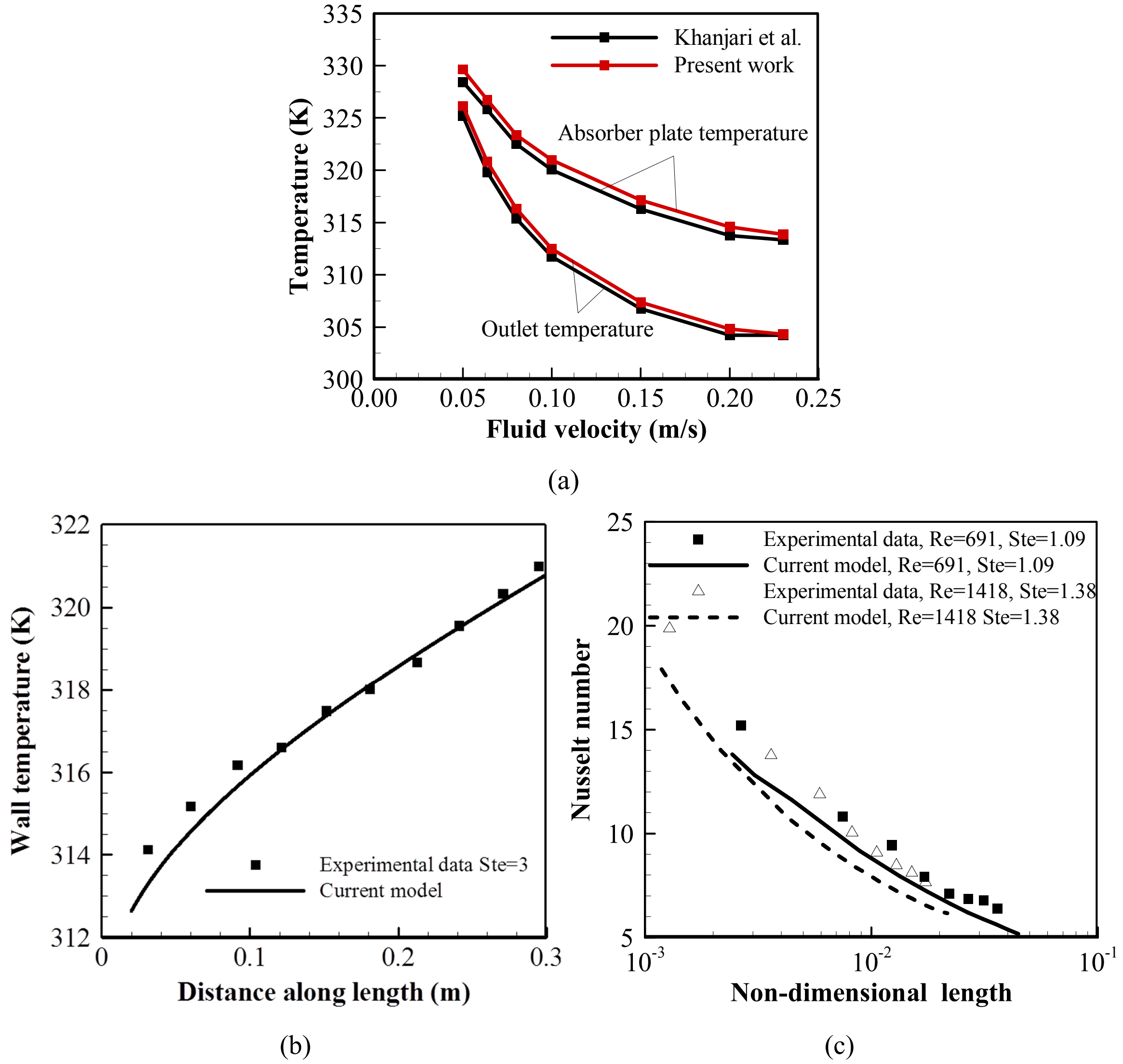

Fig. 3 Comparison with references for model validation: (a) with the results of Khanjari et al. [20]; (b) with the experimental data of Goel et al. [42]; and (c) with the experimental data of Chen et al. [35].

4. Results and discussions

4.1. Effects of MPCM volumetric concentration

To ascertain the effects of MPCM volumetric concentration in the slurry on the performance of the PV/T module under various tube inlet velocities, three different concentration values of 5%, 10% and 20% were selected for comparison while the inlet velocity varied from 0.04 m/s to 0.25 m/s. The comparisons among the three typical concentrations are enough to reveal the effects of concentration on the module performance. Therefore, only the results under the three concentrations were presented. With regards to concentrations greater than 25%, the rheological behavior of the slurry is unknown, and the viscosity could be too large to act as an effective working fluid. Hence, concentrations higher than 25% were not considered in this paper. The pure water (i.e. the MPCM concentration is 0%) was also selected as a baseline. In order to ensure that the sizes of required HTF storage tanks were the same under the same tube inlet conditions, the inlet velocity was selected instead of the mass flow rate. Fig. 4(a) shows a typical temperature distribution of the absorber plate when the slurry with c=5% enters the tube at u_{in}=0.04 m/s. It is easily observed that the temperature increases both from the plate centre to the edge and from the tube inlet to the outlet. This is because the edge of the absorber plate is far away from the cooling tube and the temperature of HTF is gradually elevated along the flow direction through continuous heat absorption. There is no sufficient cooling ability at the edge of the absorber plate, especially near the outlet, which is the intrinsic disadvantage of the plate and tube design [20]. Excess temperatures thus occur at the edge of the absorber plate near the outlet. To avoid the overheating of the PV panel at this location, the PV panel is not paved here, i.e. the PV panel is shorter than the absorber plate near the outlet as shown in Fig. 1(a). More simulations indicate that other selected concentrations and inlet velocities also offered the similar temperature distribution characteristics. The area-averaged temperature on the absorber plate surface was used to represent the absorber plate temperature in the following. Fig. 4(b) illustrates typical conversion ratios of solar radiation energy under various inlet velocities at c = 5%. The solar radiation energy is converted into three parts, which are electricity, heat dissipated into the ambient by air convection and radiation, and heat absorbed by the HTF. The ratio of solar radiation converted into electricity is the lowest among the three manners and slightly increases with the inlet velocity. The ratio dissipated into the ambient notably decreases with the increase of the inlet velocity. Therefore, the ratio absorbed by the HTF increases with the inlet velocity, which is about 61%~71%. This indicates that most solar radiation has been converted into useful heat and meanwhile the HTF plays a dominated role in the cooling.

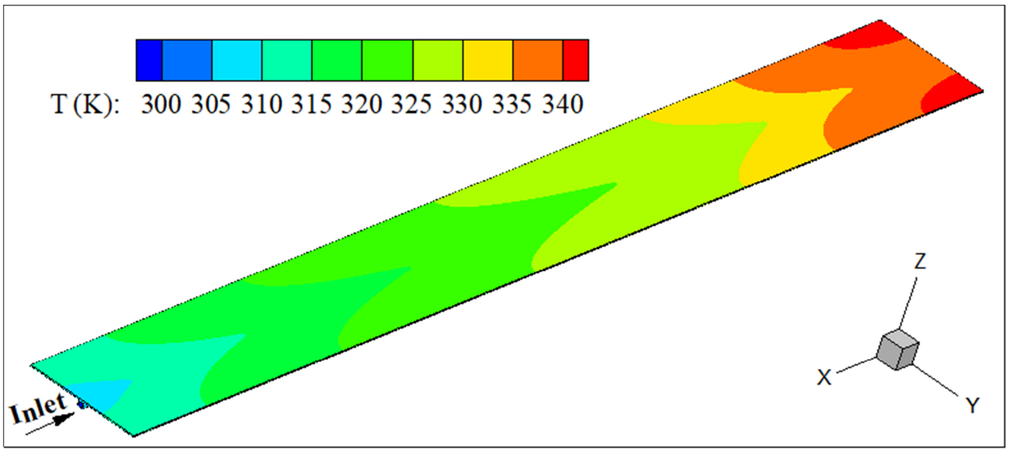

(a)

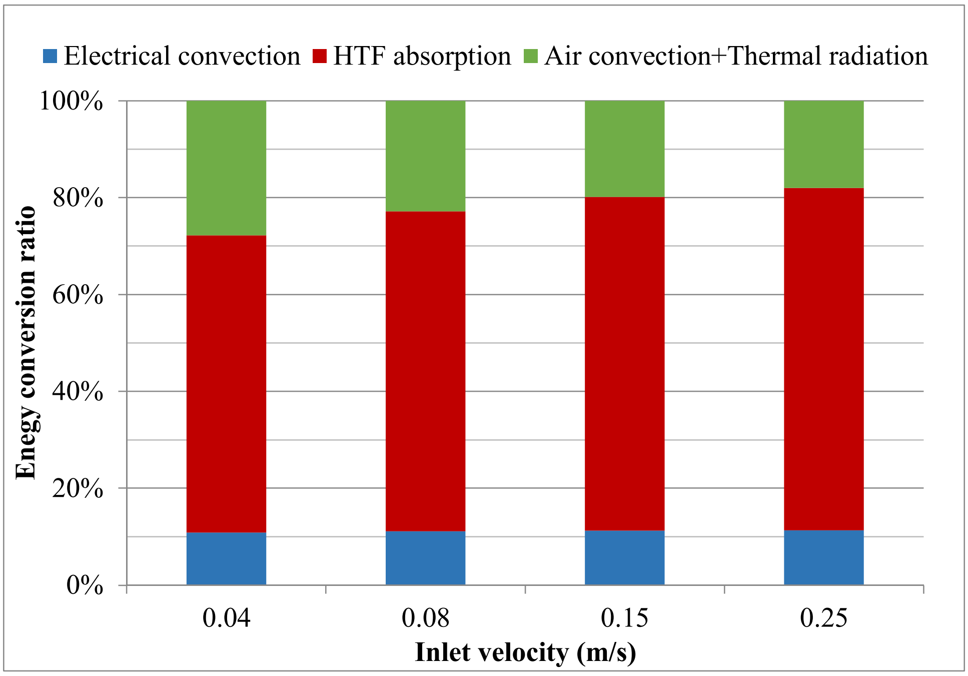

(b)

Fig. 4 Temperature distribution of the absorber plate at c=5% and u_{in}=0.04 m/s (a) and conversion ratio of solar radiation energy in the PV/T module at c=20% (b).

The temperature distributions of Section A-A under various MPCM concentrations and inlet velocities are summarized in Fig. 5. For the convenience of observation, the images are scaled by X:Z=1:100. It is obvious that the increase of inlet velocity or MPCM concentration is beneficial to obtaining a more uniform temperature distribution in the absorber plate. Some of the MPCM particles were gradually melted along the flow direction of slurry. The fluid region inside the tube can be divided into three regions: non-melting region, melting region and fully-melted region. As the inlet velocity or the MPCM concentration increases, the melting region inside the tube moves from the inlet to the outlet and the fully-melted regions are diminished. The change can be explained as follows: On one hand, as the inlet velocity increases at the same concentration, the heat absorption capacity of the HTF augments under the same temperature rise. On the other hand, the increase of MPCM concentration enhances the thermal conduction ability of the HTF, making the heat from the absorber plate to be more easily transferred to the HTF near the tube centerline. Both aspects lead to the decrease of the HTF temperature rise near the tube wall after the cold HTF flows into the tube and thus the initiating position of melting moves downstream. The changes of the melting region will lead to different melting ratios and absorbed amounts of latent heat in the tube. At a small inlet velocity (e.g. 0.04 m/s), all of the MPCM particles are fully melted in the tube at c = 5% and 10%, while a small part of the MPCM particles are not fully melted in the tube at c = 20% because the high concentration of MPCM significantly increases the latent heat absorption ability of the HTF. At a large inlet velocity (such as 0.10 m/s or 0.25 m/s), only a part of the MPCM particles for all concentrations can be totally melted, because most heat from the absorber plate is absorbed in the form of sensible heat. It can be inferred that the fully melted status for all MPCM particles can be achieved just at the outlet by adjusting the inlet velocity. The required critical inlet velocity decreases as the concentration increases. Since the absorbed amounts of latent heat and sensible heat are markedly different under various combinations of the MPCM concentration and inlet velocity, different temperature rises of fluids, cooling abilities for the PV plane, amounts of absorbed energy and exergy are caused.

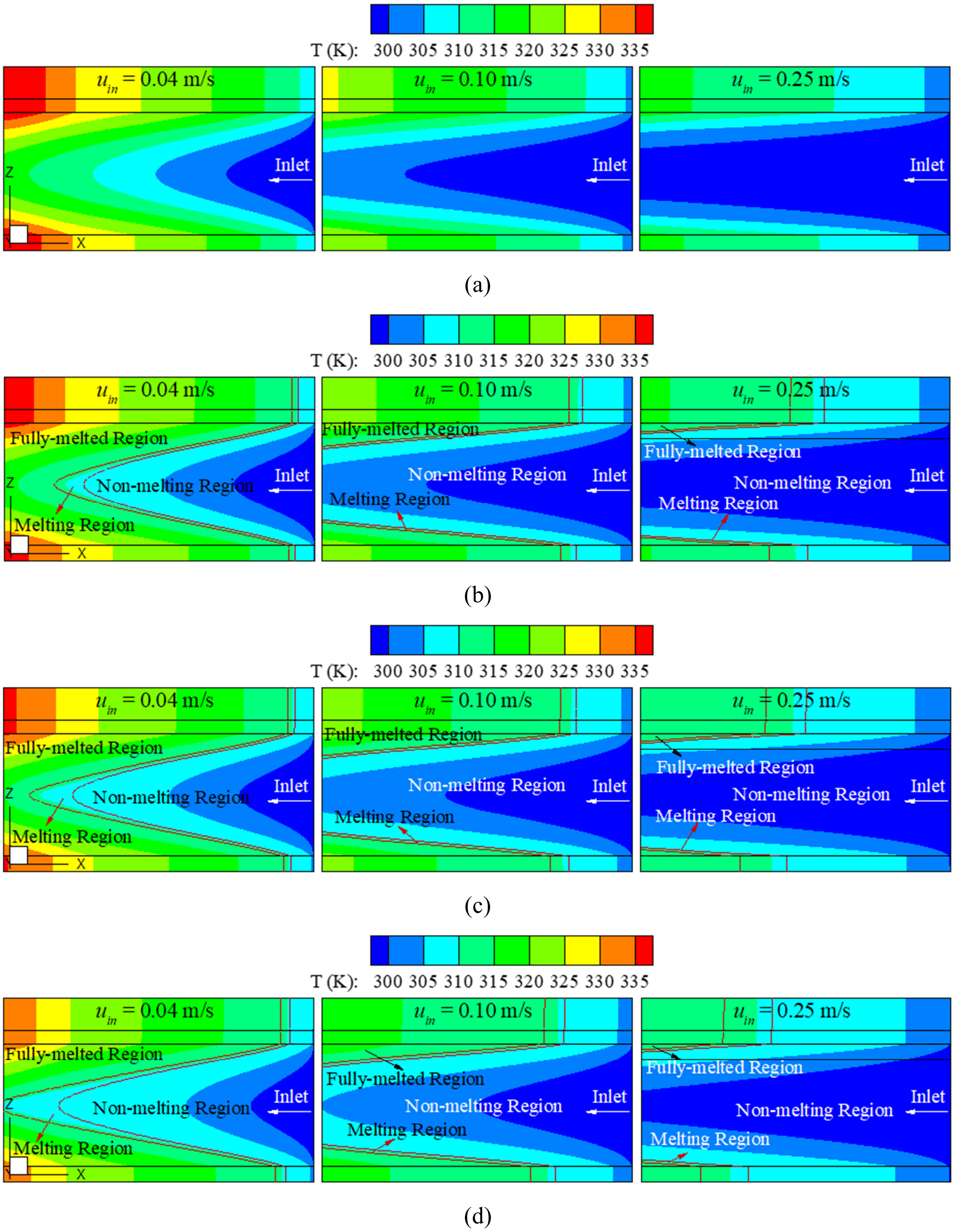

Fig. 5 Temperature distribution of Section A-A (X:Z=1:100) with different HTFs: (a) pure water; (b) slurry with *c*=5%; (c) slurry with *c*=10%; and (d) slurry with *c*=20%.

Fig. 6(a) displays the variations of outlet temperature with the inlet velocity under various HTFs and the outlet temperature drop of slurry compared with pure water at the same inlet velocity. For all volumetric concentrations, the outlet temperature decreases with the increase in the inlet velocity. The inlet velocity should be well controlled to avoid component damages or HTF evaporation caused by high temperature. Compared with pure water, the outlet temperature of slurry is lower at a low inlet velocity (<0.15 m/s) but higher at a high inlet velocity. This is because most of the MPCM particles can be melted at a small inlet velocity and the absorption of latent heat prevents a temperature rise. On the contrary, most of the MPCM particles are not melted at a large inlet velocity and they only play a role in heat transfer enhancement. Similarly, at a small inlet velocity the outlet temperature decreases with the increase of the MPCM concentration while the situation is inverse at a large inlet velocity. For a small MPCM concentration (5% or 10%), the outlet temperature drop of slurry compared with pure water has a maximum in the inlet velocity range of 0.04-0.25 m/s. Combined with Fig. 5, it can be inferred that the maximum is achieved when the MPCM particles reach the upper melting temperature at the tube outlet. In this condition, the ratio of absorbed latent heat to sensible heat of the HTF in the tube is greatest. The variations of average temperature of the absorber plate with the inlet velocity under various HTFs are shown in Fig. 6(b). Obviously the higher inlet velocity and larger MPCM concentration exhibit stronger cooling ability for the PV panel. The reason is that the HTF with a larger MPCM concentration can absorb more heat in a small temperature rise via latent heat absorption. Fig. 6(b) also illustrates the temperature drops of absorber plate under the slurries with respect to pure water at the same inlet velocity. The slurry with the MPCM concentration of 20% can lower the absorber plate temperature by 2.4 K~4.4 K compared to the pure water in the selected inlet velocity range. The enhancement of cooling ability of MPCM slurry compared to pure water decrease with the increasing inlet velocity, which is due to the reduction in the ratio of absorbed latent heat to sensible heat of the HTF.

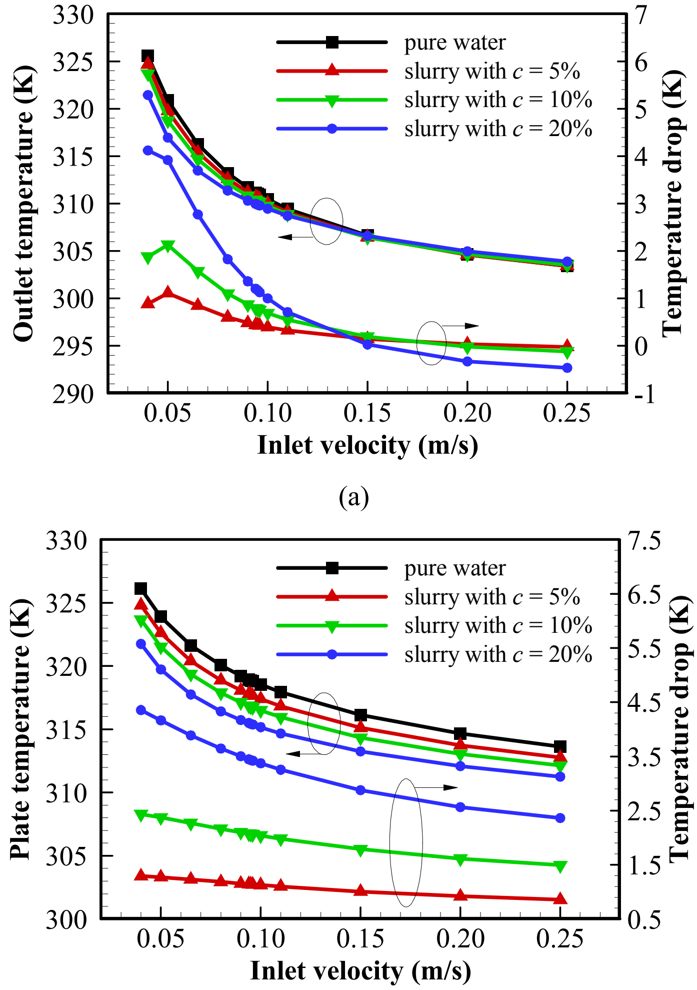

(a)

(b)

Fig. 6 Temperature variation with inlet velocity at different MPCM volumetric concentrations: (a) outlet; and (b) absorber plate. The temperature drop is calculated with respect to pure water at the same inlet velocity.

As previously described, the utilization of HTFs at the back of the PV panel is designed to simultaneously capture thermal energy for use and cool the PV panel for preventing electrical efficiency loss. Hence, the thermal and electrical efficiencies are two very crucial parameters to indicate the PV/T module performance. The variations in thermal and electrical efficiencies with the inlet velocity for different MPCM concentrations are demonstrated in Fig. 7(a). Increasing the inlet velocity or MPCM concentration can both augment the thermal efficiency. The thermal energy from solar radiation is partially captured by the HTF and partially dissipated to the environment by air convection and thermal radiation. With the increase in inlet velocity or MPCM concentration, the temperature of the absorber plate or PV panel decreases as demonstrated in Fig. 6(b). Subsequently, the thermal energy dissipated to the environment decreases and more thermal energy is captured by the HTF for use, as presented in Fig. 4(b). Therefore, the thermal efficiency increases. According to Eq. (12), since the increase of the inlet velocity or MPCM concentration results in the reduction of the PV panel temperature, the electrical efficiency accordingly increases. The overall performance of the module is characterized by the primary-energy saving efficiency defined in Eq. (13). The variations of the primary-energy saving efficiency for various HTFs versus the inlet velocity are illustrated in Fig. 7(b). Since the thermal and electrical efficiencies are both increased, the primary-energy saving efficiency increases with the MPCM concentration or inlet velocity. The increasing rate of the efficiency progressively decreases with the increasing inlet velocity for each HTF. The relative primary-energy saving efficiency increments for the slurries with respect to the pure water at the same inlet velocity are also illustrated in Fig. 7(b). It is apparent that the slurries provide larger efficiency improvement at smaller inlet velocities with respect to the pure water. Specifically, the slurry with c = 20% results in a relative increment of 2.5%~5.7% in the primary-energy saving efficiency in the selected inlet velocity range.

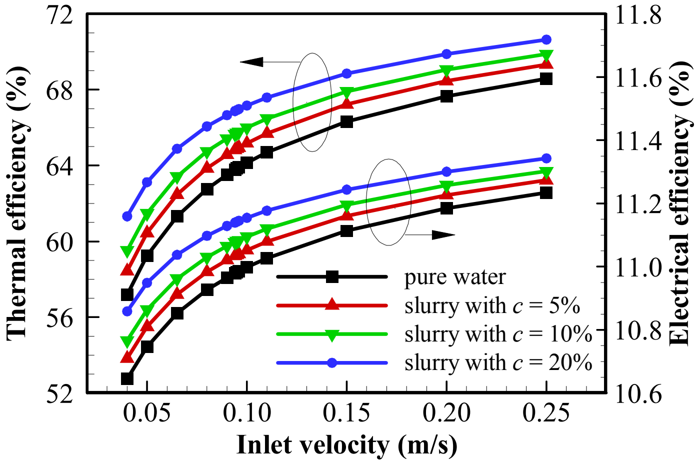

(a)

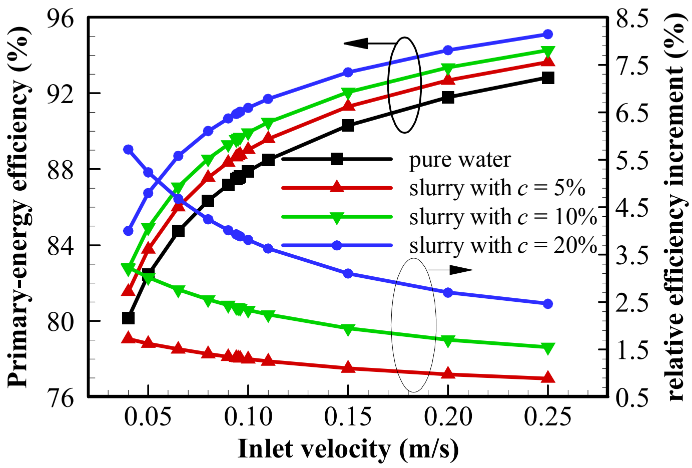

(b)

Fig. 7 Variations with inlet velocity at different MPCM volumetric concentrations: (a) thermal efficiency and electrical efficiency; (b) primary-energy saving efficiency and relative efficiency increment with respect to pure water at the same inlet velocity.

The quality of captured energy can be indicated by thermal exergy and electrical exergy. Fig. 8(a) presents the variations of thermal exergy and electrical exergy captured by the whole PV/T module for various HTFs with the inlet velocity. It can be found that the thermal exergy decreases with the increasing inlet velocity because more heat is absorbed at lower temperatures. For example, the thermal exergy for the slurry with c = 20% decreases from about 58 W to 33 W when the inlet velocity increases from 0.04 m/s to 0.25 m/s. At low inlet velocities, the thermal exergy of slurry is lower compared to pure water; when the inlet velocity increases over about 0.065 m/s the former becomes larger than the latter; with the further increase in the inlet velocity, the difference between the two gradually diminishes. Moreover, the thermal exergy increases with the MPCM concentration in the inlet velocity range of 0.065~0.25 m/s, which is the same as the thermal efficiency. The trend can be explained as follows: More sensible heat is absorbed at temperatures greater than the MPCM melting temperature for pure water at small inlet velocities. On the contrary at large inlet velocities, the heat absorption temperature of the pure water decreases and more latent heat is absorbed near the relatively high MPCM melting temperature for the slurries; meanwhile, the larger the MPCM concentration, the more the absorbed latent heat. Further increasing the inlet velocity results in the notable decrease in the ratio of absorbed latent heat to sensible heat, and thus the contribution of absorbed latent heat to the thermal exergy is reduced. The electrical exergy increases with the inlet velocity or MPCM concentration, which is the same as the change trend of the electrical efficiency. Specifically, the electrical exergy for the slurry with c = 20% increases from about 178 W to 186 W when the inlet velocity increases from 0.04 m/s to 0.25 m/s, which is notably greater than the thermal exergy at the same conditions. Moreover, the improvement of electrical efficiency by increasing the MPCM concentration is gradually weakened with the increase in the inlet velocity.

The ability to capture available energy of the PV/T module from the solar radiation is indicated by the exergy efficiency. The variations of exergy efficiency with the inlet velocity for different MPCM concentrations are presented in Fig. 8(b). The exergy efficiency generally decreases with the increase of inlet velocity, which is opposite to the trend of primary-energy saving efficiency as presented in Fig. 7(b). This is caused by the remarkable reduction of the thermal exergy. Like the primary-energy saving efficiency, the increase of MPCM concentration is still able to increase the exergy efficiency, which is mainly attributed to the increase of electrical exergy. The variation rate of exergy efficiency for the slurries with the inlet velocity is lower than the pure water. The relative exergy efficiency increment of the slurry versus the pure water is also illustrated in Fig. 8(b). The slurries with different MPCM concentrations exhibit similar variation characteristics of relative exergy efficiency increment, which first increases and then decreases as the inlet velocity increases. The maximum point becomes higher and the variation becomes more dramatic with the increase in the concentration. The reason is that the higher the concentration, the larger the variations in absorbed latent heat and entropy generation caused by flow friction for the same inlet velocity change. The maximum exergy efficiency increments for the slurries with c = 5%, 10% and 20% are 0.61%, 1.16% and 2.14%, respectively. The corresponding inlet velocities are 0.01 m/s, 0.096 m/s and 0.095 m/s, respectively. This implies that the addition of MPCM achieves the optimum enhancement in the PV/T module performance at these inlet velocities.

Compared to the work of Khanjari et al. [20], the exergy efficiency obtained in this study is lower. The reasons are as follows: On one hand, Khanjari et al. [20] did not consider the heat dissipation caused by the ambient air convection and ambient radiation in their model, which is different from the present study; It means that all of the heat produced by solar radiation was absorbed by the HTF in their simulations. On the other hand, the solar radiation intensity was set as 800 W/m^2 in the work of Khanjari et al. [20], less than the set value of 1000 W/m^2 in the present study; Liu et al. [32] indicated that a lower solar radiation intensity gave rise to greater electrical and thermal efficiencies. Furthermore, the exergy efficiency obtained in this study is higher compared with the work of Liu et al. [31], although the solar radiation intensity was lower (589-852 W/m^2) in their work.

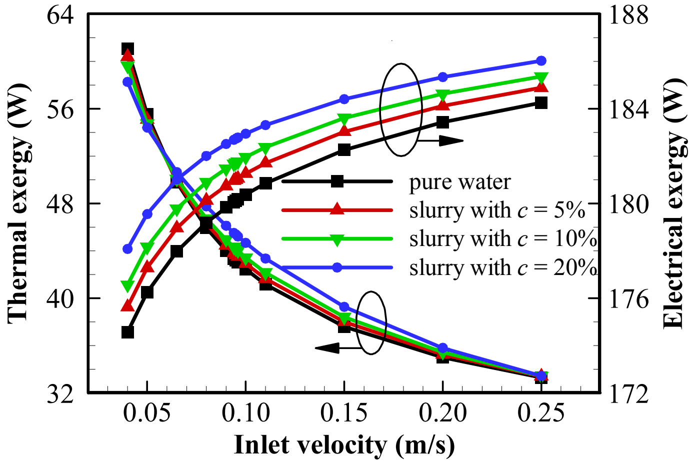

(a)

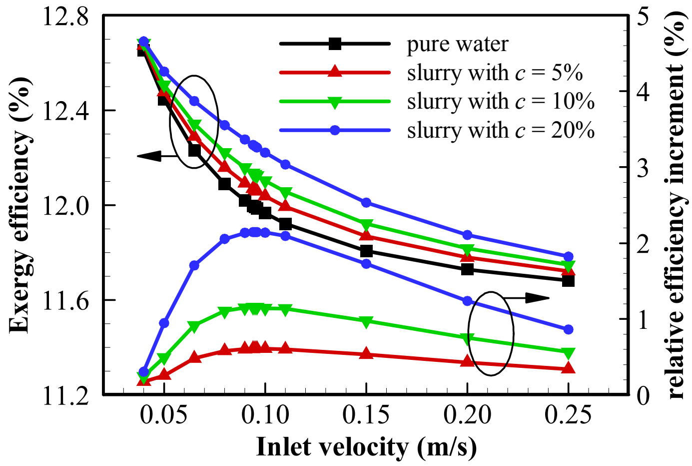

(b)

Fig. 8 Variations with inlet velocity at different MPCM volumetric concentrations: (a) thermal exergy and electrical exergy; (b) exergy efficiency and increment compared to pure water at the same inlet velocity.

4.2. Effects of MPCM melting temperature

To ascertain the effects of MPCM melting temperature on the PV/T module performance, three different melting temperatures, i.e. 27 °C, 37 °C and 47 °C, were selected in the study for comparison, which are in the achievable operation temperature range of the PV/T module. The MPCM concentration was set to 20% in this section. Fig. 9 summarizes the temperature distributions of Section A-A under various melting temperatures with different inlet velocities. With the increase of melting temperature, the melting region moves from the tube inlet to the outlet and the absorber plate exhibits more uneven temperature distribution at the same inlet velocity. Under the small inlet velocity (e.g. 0.04 m/s), only the melting temperature of 27°C ensures that all of the MPCM particles are fully melted in the tube. Lower inlet velocities are required to achieve this situation for the other two higher melting temperatures. Under the inlet velocity of 0.25 m/s, no melting of MPCM occurs in the tube for T_m = 47 °C.

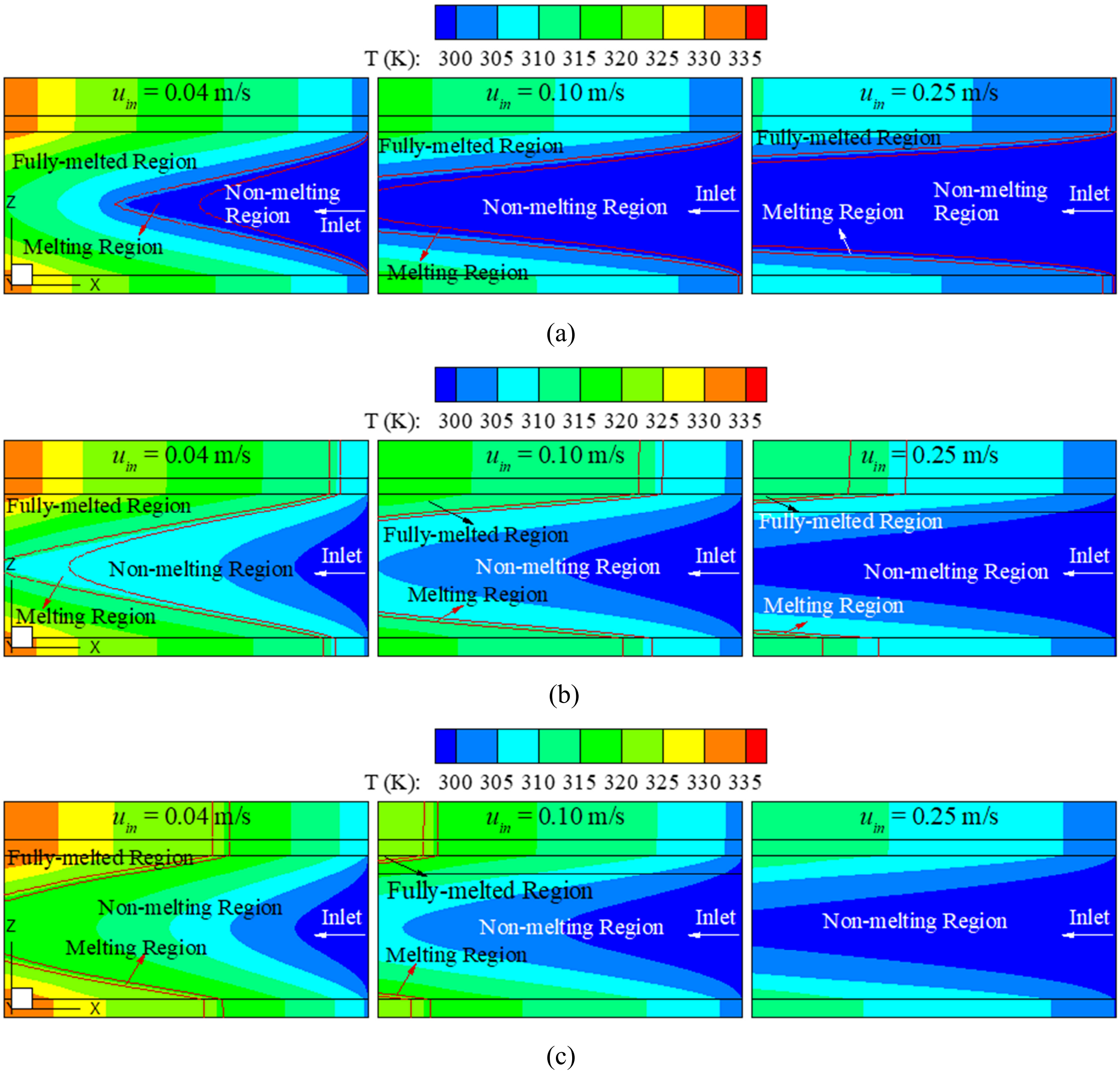

Fig. 9 Temperature distribution of Section A-A (X:Z=1:100) using slurry with different melting temperatures: (a) 27 °C; (b) 37 °C; and (c) 47 °C.

Fig. 10(a) displays the variations of outlet temperature of slurries with various melting temperatures versus the inlet velocity. The outlet temperature of slurry with T_m = 27°C is always lower compared to pure water in the whole selected range of inlet velocity, while this situation is changed for the other two higher melting temperatures at high inlet velocities. This is because the main role of the MPCM particles gradually shifts from absorbing latent heat to enhancing heat transfer ability for the two higher melting temperatures with the increase in inlet velocity. Fig. 10(a) also shows the outlet temperature drops of slurries with respect to pure water at the same inlet velocity. Different melting temperatures lead to totally different variation characteristics of the outlet temperature drop with the inlet velocity compared to pure water. The temperature drop first increases and then decreases for T_m = 27°C while the change trend is inverse for T_m = 47°C. The variations of average temperature of the absorber plate with the inlet velocity under various MPCM melting temperatures are demonstrated in Fig. 10(b). Obviously, the slurry with a lower MPCM melting temperature leads to lower absorber plate temperatures, and thus shows stronger cooling ability for the PV panel. This can be explained by the fact that a lower MPCM melting temperature ensures that more heat is absorbed by the HTF at a lower temperature. Fig. 10(b) also shows the temperature drops of the absorber plate for slurries compared with pure water. The temperature drop of absorber plate exhibits a similar change trend to the outlet temperature drop as presented in Fig. 10(a). The slurry with T_m = 27°C has highest the cooling ability among the three melting temperatures, which can lower the absorber plate temperature by 5.2 K~6.3 K compared to pure water at the selected inlet velocity range. Its maximum cooling ability enhancement occurs at the inlet velocity of about 0.06 m/s.

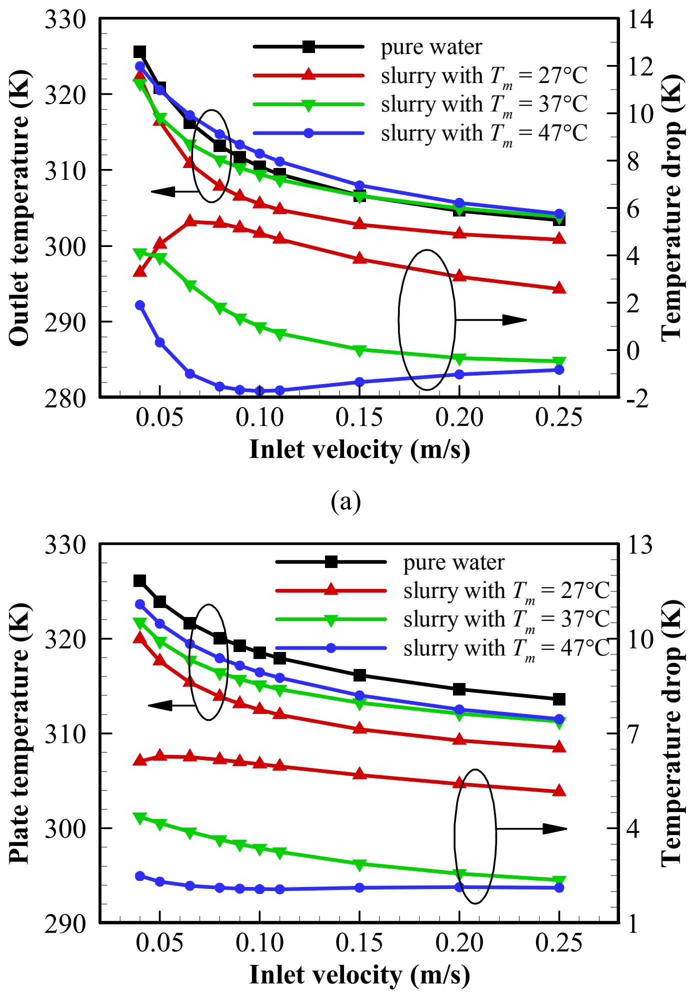

(a)

(b)

Fig. 10 Temperature variation with inlet velocity at different MPCM melting temperatures: (a) outlet; and (b) absorber plate. The temperature drop is calculated with respect to pure water at the same inlet velocity.

The variations of thermal and electrical efficiencies with the inlet velocity for various melting temperatures are demonstrated in Fig. 11(a). It is apparent that decreasing the MPCM melting temperature can augment both the thermal and electrical efficiencies. This is directly attributed to the lower absorber plate temperature at a lower melting temperature as shown in Fig. 10(b). The lower absorber plate leads to less heat dissipation into the ambient by air convection and radiation and more heat is absorbed by the HTF, which accordingly results in high thermal efficiency. Moreover, the lower absorber plate means lower PV panel temperature and thus higher electrical efficiency. The primary-energy saving efficiencies calculated based on thermal and electrical efficiencies for various melting temperatures are illustrated in Fig. 11(b). Since the thermal and electrical efficiencies are both increased with the decrease in melting temperature, a lower melting temperature results in a higher the primary-energy saving efficiency. It is worth noting that the selected melting temperature should be higher than the inlet HTF temperature. Moreover, all the slurries with the three different melting temperatures offer higher primary-energy saving efficiency than the pure water. The relative increment in the primary-energy saving efficiency for slurries with respect to pure water is also presented in Fig. 11(b). The relative efficiency increment notably decreases with the increase of the inlet velocity for T_m = 27℃ and 37℃, whereas it keeps relatively constant for the melting temperature of 47℃. Among the three melting temperatures, the slurry with T_m = 27℃ obtains the largest improvement in the primary-energy saving efficiency versus the pure water, which results in a relative increment of 5.6%~8.3% at the selected inlet velocity range.

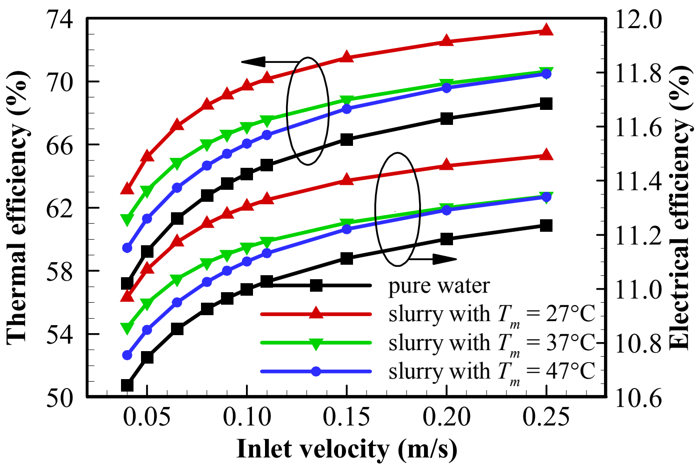

(a)

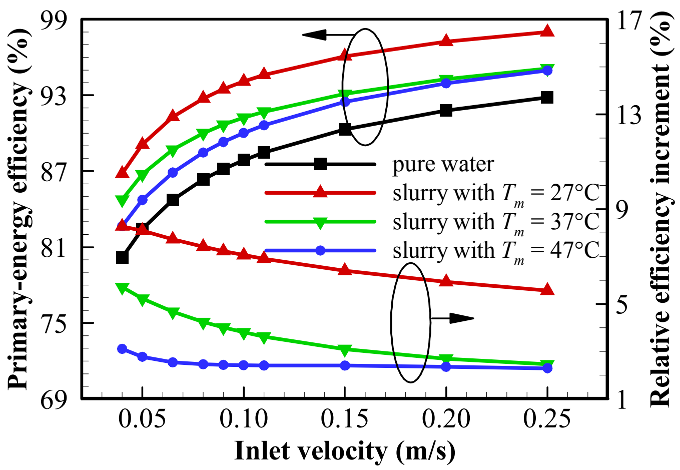

(b)

Fig. 11 Variations with inlet velocity at different MPCM melting temperatures: (a) thermal efficiency and electrical efficiency; (b) primary-energy saving efficiency and relative efficiency increment with respect to pure water at the same inlet velocity.

The variations of thermal exergy and electrical exergy captured by the PV/T module with the inlet velocity at various melting temperatures are presented in Fig. 12(a). Compared to pure water at the same inlet velocity, the slurry with T_m = 27°C captures much less thermal exergy because more heat is absorbed at such a low melting temperature, while the slurry with T_m = 47°C captures more thermal exergy at small inlet velocities but the improvement gradually diminishes until it vanishes with the increase of the inlet velocity. They are different from the situation for the slurry with T_m = 37°C. The slurry provides higher electrical exergy than pure water at the same inlet velocity regardless of the melting temperature, and the electrical exergy increases as the melting temperature decreases due to the resulting lower absorber plate temperature.

The variations of exergy efficiency with the inlet velocity for various melting temperatures are shown in Fig. 12(b). Compared to the pure water at the same inlet velocity, the exergy efficiency for the slurry with T_m = 27°C is less, while those for the slurries with T_m = 37°C and 47°C are higher. Although the electrical exergy is largest for the melting temperature of 27°C, the thermal exergy is lowest and the sum of the two exergies is lowest, which leads to the lowest exergy efficiency. Furthermore, the exergy efficiency for the slurry with T_m = 47°C is larger than that for the slurry with T_m = 37°C at small inlet velocities, while the former is less at large inlet velocities. The variations of the relative exergy efficiency increment of the slurries with respect to the pure water are also illustrated in Fig. 12(b). Likewise, the relative exergy efficiency increments for all the slurries with various melting temperatures have extremums in the selected inlet velocity range. The maximum relative exergy efficiency increments for the slurries with T_m = 37 °C and 47 °C are 2.14% and 3.23%, respectively. They occur at the inlet velocities of 0.095 m/s and 0.05m/s, respectively. From the above, adding the MPCM with T_m = 47°C into the pure water can achieve the largest enhancement in the exergy efficiency of the module among the three melting temperatures, while the exergy efficiency is largely weakened at T_m = 27°C instead.

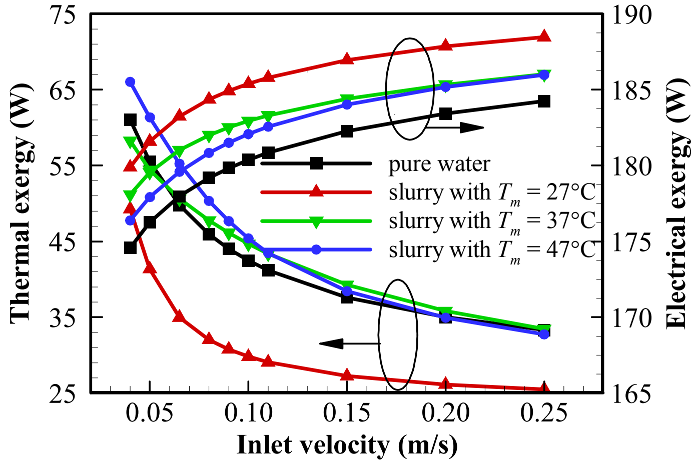

(a)

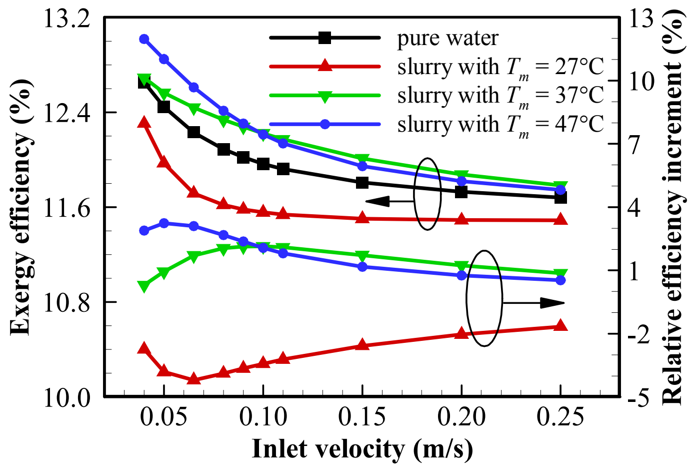

(b)

Fig. 12 Variations with inlet velocity at different MPCM melting temperatures: (a) thermal exergy and electrical exergy; (b) exergy efficiency and increment compared to pure water at the same inlet velocity.

5. Conclusions

A numerical model of coupled heat transfer was established to examine the performance of a MPCM slurry based PV/T module in this study. This model allowed for the photoelectric conversion, HTF flow, air convection and ambient radiation. The effects of MPCM volumetric concentration and melting temperature on the energy efficiency and exergy efficiency of the module in a wide inlet velocity range were explored in detail. On the basis of the simulation results, the main conclusions can be obtained as follows:

(1) The increase of volumetric concentration of MPCM particles simultaneously elevated the electrical and thermal efficiencies as well as exergy efficiency under a relatively high MPCM melting temperature.

(2) Both the electrical and thermal efficiencies increased with the decrease in MPCM melting temperature, whereas higher melting temperatures (47°C) should be selected to obtain preferable exergy efficiency. The slurry with an excessively low melting temperature (27°C) even resulted in lower exergy efficiency than pure water due to lower thermal exergy.

(3) Compared with pure water, the slurry provided a greater improvement in energy efficiency at a lower inlet velocity, whilst the maximum improvement in exergy efficiency was achieved at a certain inlet velocity. The maximum improvements in energy and exergy efficiencies were 8.3% and 3.23% among the selected parameter ranges, respectively.

Acknowledgement

The authors would like to acknowledge the financial support of the Engineering and Physical Sciences Research Council (EPSRC) of the United Kingdom (Grant Nos. EP/N000714/1 and EP/N021142/1), National Natural Science Foundation of China (Grant Nos. 51606135 and 51776142) and Natural Science Foundation of Hubei Province (Grant No. 2016CFB156).

References

[1] Y. Du, C.J. Fell, B. Duck, D. Chen, K. Liffman, Y. Zhang, et al. Evaluation of photovoltaic panel temperature in realistic scenarios. Energy Convers Manage 108 (2016) 60-7.

[2] O. Dupré, R. Vaillon, M.A. Green. Physics of the temperature coefficients of solar cells. Sol Energy Mater Sol Cells 140 (2015) 92-100.

[3] E. Skoplaki, J.A. Palyvos. On the temperature dependence of photovoltaic module electrical performance: A review of efficiency/power correlations. Sol Energy 83 (2009) 614-24.

[4] S. Singh, S. Agrawal, D.V. Avasthi. Design, modeling and performance analysis of dual channel semitransparent photovoltaic thermal hybrid module in the cold environment. Energy Convers Manage 114 (2016) 241-50.

[5] S. Bhattarai, J.-H. Oh, S.-H. Euh, G. Krishna Kafle, D. Hyun Kim. Simulation and model validation of sheet and tube type photovoltaic thermal solar system and conventional solar collecting system in transient states. Sol Energy Mater Sol Cells 103 (2012) 184-93.

[6] F. Shan, F. Tang, L. Cao, G. Fang. Comparative simulation analyses on dynamic performances of photovoltaic–thermal solar collectors with different configurations. Energy Convers Manage 87 (2014) 778-86.

[7] Z. Qiu, X. Ma, X. Zhao, P. Li, S. Ali. Experimental investigation of the energy performance of a novel Micro-encapsulated Phase Change Material (MPCM) slurry based PV/T system. Appl Energy 165 (2016) 260-71.

[8] X. Zhang, X. Zhao, S. Smith, J. Xu, X. Yu. Review of R&D progress and practical application of the solar photovoltaic/thermal (PV/T) technologies. Renew Sust Energ Rev. 16 (2012) 599-617.

[9] M. Farshchimonfared, J.I. Bilbao, A.B. Sproul. Channel depth, air mass flow rate and air distribution duct diameter optimization of photovoltaic thermal (PV/T) air collectors linked to residential buildings. Renew Energy. 76 (2015) 27-35.

[10] S.C. Solanki, S. Dubey, A. Tiwari. Indoor simulation and testing of photovoltaic thermal (PV/T) air collectors. Appl Energy 86 (2009) 2421-8.

[11] N. Dimri, A. Tiwari, G.N. Tiwari. Thermal modelling of semitransparent photovoltaic thermal (PVT) with thermoelectric cooler (TEC) collector. Energy Convers Manage 146 (2017) 68-77.

[12] A. Habibollahzade. Employing photovoltaic/thermal panels as a solar chimney roof: 3E analyses and multi-objective optimization. Energy. 166 (2019) 118-30.

[13] J. Zhang, Y. Xuan, L. Yang. Performance estimation of photovoltaic–thermoelectric hybrid systems. Energy. 78 (2014) 895-903.

[14] N. Aste, F. Leonforte, C. Del Pero. Design, modeling and performance monitoring of a photovoltaic–thermal (PVT) water collector. Sol Energy 112 (2015) 85-99.

[15] C.-F.J. Kuo, J.-M. Liu, M.L. Umar, W.-L. Lan, C.-Y. Huang, S.-S. Syu. The photovoltaic-thermal system parameter optimization design and practical verification. Energy Convers Manage 180 (2019) 358-71.

[16] S. Mousavi, A. Kasaeian, M.B. Shafii, M.H. Jahangir. Numerical investigation of the effects of a copper foam filled with phase change materials in a water-cooled photovoltaic/thermal system. Energy Convers Manage 163 (2018) 187-95.

[17] K. Thinsurat, H. Bao, Z. Ma, A.P. Roskilly. Performance study of solar photovoltaic-thermal collector for domestic hot water use and thermochemical sorption seasonal storage. Energy Convers Manage 180 (2019) 1068-84.

[18] M. Sardarabadi, M. Passandideh-Fard, S. Zeinali Heris. Experimental investigation of the effects of silica/water nanofluid on PV/T (photovoltaic thermal units). Energy. 66 (2014) 264-72.

[19] A. Kasaeian, A.T. Eshghi, M. Sameti. A review on the applications of nanofluids in solar energy systems. Renew Sust Energ Rev. 43 (2015) 584-98.

[20] Y. Khanjari, F. Pourfayaz, A.B. Kasaeian. Numerical investigation on using of nanofluid in a water-cooled photovoltaic thermal system. Energy Convers Manage 122 (2016) 263-78.

[21] M.O. Lari, A.Z. Sahin. Design, performance and economic analysis of a nanofluid-based photovoltaic/thermal system for residential applications. Energy Convers Manage 149 (2017) 467-84.

[22] K. Rahbar, A. Riasi, H. Khatam Bolouri Sangjoeei, N. Razmjoo. Heat recovery of nano-fluid based concentrating Photovoltaic Thermal (CPV/T) Collector with Organic Rankine Cycle. Energy Convers Manage 179 (2019) 373-96.

[23] E. Bellos, C. Tzivanidis. Investigation of a nanofluid-based concentrating thermal photovoltaic with a parabolic reflector. Energy Convers Manage 180 (2019) 171-82.

[24] Q. Yu, F. Tchuenbou-Magaia, B. Al-Duri, Z. Zhang, Y. Ding, Y. Li. Thermo-mechanical analysis of microcapsules containing phase change materials for cold storage. Appl Energy 211 (2018) 1190-202.

[25] G. Zhang, G. Cui, B. Dou, Z. Wang, M.A. Goula. An experimental investigation of forced convection heat transfer with novel microencapsulated phase change material slurries in a circular tube under constant heat flux. Energy Convers Manage 171 (2018) 699-709.

[26] Y. Allouche, S. Varga, C. Bouden, A.C. Oliveira. Experimental determination of the heat transfer and cold storage characteristics of a microencapsulated phase change material in a horizontal tank. Energy Convers Manage 94 (2015) 275-85.

[27] N.S. Roberts, R. Al-Shannaq, J. Kurdi, S.A. Al-Muhtaseb, M.M. Farid. Efficacy of using slurry of metal-coated microencapsulated PCM for cooling in a micro-channel heat exchanger. Appl Therm Eng 122 (2017) 11-8.

[28] Z. Qiu, X. Ma, P. Li, X. Zhao, A. Wright. Micro-encapsulated phase change material (MPCM) slurries: Characterization and building applications. Renew Sust Energ Rev. 77 (2017) 246-62.

[29] L. Liu, G. Alva, Y. Jia, X. Huang, G. Fang. Dynamic thermal characteristics analysis of microencapsulated phase change suspensions flowing through rectangular mini-channels for thermal energy storage. Energy and Buildings. 134 (2017) 37-51.

[30] Z. Qiu, X. Zhao, P. Li, X. Zhang, S. Ali, J. Tan. Theoretical investigation of the energy performance of a novel MPCM (Microencapsulated Phase Change Material) slurry based PV/T module. Energy. 87 (2015) 686-98.

[31] L. Liu, Y. Jia, Y. Lin, G. Alva, G. Fang. Performance evaluation of a novel solar photovoltaic–thermal collector with dual channel using microencapsulated phase change slurry as cooling fluid. Energy Convers Manage 145 (2017) 30-40.

[32] L. Liu, Y. Jia, Y. Lin, G. Alva, G. Fang. Numerical study of a novel miniature compound parabolic concentrating photovoltaic/thermal collector with microencapsulated phase change slurry. Energy Convers Manage 153 (2017) 106-14.

[33] F. Bai, M. Chen, W. Song, Q. Yu, Y. Li, Z. Feng, et al. Investigation of thermal management for lithium-ion pouch battery module based on phase change slurry and mini channel cooling plate. Energy. 167 (2019) 561-74.

[34] P. Charunyakorn, S. Sengupta, S.K. Roy. Forced convection heat transfer in microencapsulated phase change material slurries: flow in circular ducts. Int J Heat Mass Transf. 34 (1991) 819-33.

[35] B. Chen, X. Wang, R. Zeng, Y. Zhang, X. Wang, J. Niu, et al. An experimental study of convective heat transfer with microencapsulated phase change material suspension: Laminar flow in a circular tube under constant heat flux. Experimental Thermal and Fluid Science. 32 (2008) 1638-46.

[36] A.B.S. Alquaity, S.A. Al-Dini, E.N. Wang, B.S. Yilbas. Numerical investigation of liquid flow with phase change nanoparticles in microchannels. Int J Heat Fluid Flow 38 (2012) 159-67.

[37] S. Kumar, S.C. Mullick. Wind heat transfer coefficient in solar collectors in outdoor conditions. Sol Energy 84 (2010) 956-63.

[38] L. Chai, X. Wang, D. Wu. Development of bifunctional microencapsulated phase change materials with crystalline titanium dioxide shell for latent-heat storage and photocatalytic effectiveness. Appl Energy 138 (2015) 661-74.

[39] V. Vand. Theory of Viscosity of Concentrated Suspensions. Nature. 155 (1945) 364.

[40] J. Ji, J.-P. Lu, T.-T. Chow, W. He, G. Pei. A sensitivity study of a hybrid photovoltaic/thermal water-heating system with natural circulation. Appl Energy 84 (2007) 222-37.

[41] A. Bejan. Entropy generation through heat and fluid flow. Wiley1982.

[42] M. Goel, S. Roy, S. Sengupta. Laminar forced convection heat transfer in microcapsulated phase change material suspensions. Int J Heat Mass Transf. 37 (1994) 593-604.